



A Journal of the Gesellschaft Deutscher Chemiker

Angewandte Chemie

GDCh

International Edition

www.angewandte.org

Accepted Article

Title: Homolytic versus Heterolytic Hydrogen Evolution Reaction Steered via Steric Effect

Authors: Xiaojun Guo, Ni Wang, Xialiang Li, Zongyao Zhang, Jianping Zhao, Wanjie Ren, Shuping Ding, Gelun Xu, Jianfeng Li, Ulf-Peter Apfel, Wei Zhang, and Rui Cao

This manuscript has been accepted after peer review and appears as an Accepted Article online prior to editing, proofing, and formal publication of the final Version of Record (VoR). This work is currently citable by using the Digital Object Identifier (DOI) given below. The VoR will be published online in Early View as soon as possible and may be different to this Accepted Article as a result of editing. Readers should obtain the VoR from the journal website shown below when it is published to ensure accuracy of information. The authors are responsible for the content of this Accepted Article.

To be cited as: *Angew. Chem. Int. Ed.* 10.1002/anie.202002311
Angew. Chem. 10.1002/ange.202002311

Link to VoR: <http://dx.doi.org/10.1002/anie.202002311>
<http://dx.doi.org/10.1002/ange.202002311>

Homolytic versus Heterolytic Hydrogen Evolution Reaction Steered via Steric Effect

Xiaojun Guo, Ni Wang, Xialiang Li, Zongyao Zhang, Jianping Zhao, Wanjie Ren, Shuping Ding, Gelun Xu, Jianfeng Li, Ulf-Peter Apfel, Wei Zhang, and Rui Cao*

Abstract: Several H–H bond forming pathways have been proposed for the hydrogen evolution reaction (HER). Revealing these HER mechanisms is of fundamental importance for the rational design of catalysts and is also extremely challenging. Herein we report an unparalleled example of switching between homolytic and heterolytic HER mechanisms. We designed and synthesized three nickel(II) porphyrins with distinct steric effects by introducing bulky amido moieties to *ortho*- or *para*-positions of the *meso*-phenyl groups. We furthermore showed their different catalytic HER behaviors. For these Ni porphyrins, although their 1e-reduced forms are active to reduce trifluoroacetic acid, the resulted Ni hydrides – depending on the steric effects of porphyrin rings – have different pathways to make H₂. Understanding HER processes, especially controllable switching between homolytic and heterolytic H–H bond formation pathways through molecular engineering, is unprecedented in fundamentals of electrocatalysis.

The viability of a hydrogen-based energy society is depended on efficient and durable production of hydrogen.^[1–5] Recent efforts have resulted in the identification of many molecular catalysts for hydrogen evolution.^[6–36] Despite these achievements, however, understanding and further controlling reaction processes are still highly challenging.^[37,38] Metal hydrides, which can be generated through the oxidative protonation of metal ions in their reduced states,^[39–42] are usually proposed as key intermediates to evolve H₂ through homolytic or heterolytic pathways (Figure 1a).^[37,38,43] Although these reaction paradigms have long been suggested, a well-defined bimetallic homolytic HER has been rarely reported. As a consequence, switching between homolytic and heterolytic HER pathways in a controllable manner is unprecedented.

Recently, we showed that Ni^{III}–H, formed via the protonation of singly reduced Ni tetrakis(pentafluorophenyl)porphyrin (TFPF), underwent bimetallic homolysis to generate H₂.^[43] The transition

state of the homolytic H–H bond formation was located based on calculations, showing a face-to-face arrangement of the two porphyrin macrocycles (Figure 1b). Results from calculations and experiments using stopped-flow techniques suggest that the formation of Ni^{III}–H – through the protonation of Ni^I ion – is the rate-limiting step, and subsequent homolytic HER between two Ni^{III}–H is very fast. Similar bimolecular reaction of Ni^{III}–H to give H₂ has also been suggested to take place quickly (i.e., estimated $k > 10^7 \text{ M}^{-1} \text{ s}^{-1}$),^[44] making the detection of Ni^{III}–H intermediates challenging. Because of the high bimolecular reactivity of Ni^{III}–H, we propose to introduce bulky substituents on both sides of the porphyrin macrocycles to block the bimolecular mechanism.

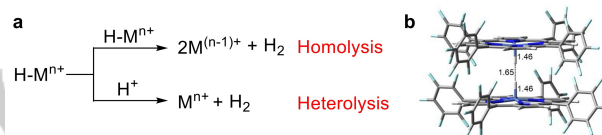


Figure 1. (a) Proposed homolytic and heterolytic HER pathways. (b) Calculated transition state of the bimetallic homolysis for the H–H bond formation mediated by Ni TFPF. Bond lengths are given in Å. Copyright 2016 Wiley-VCH.

Herein, we report the syntheses and catalytic HER features of Ni porphyrins **1–3** (Figure 2a). Their *meso*-phenyl groups bear amido moieties at *ortho*-positions for **1** and *para*-positions for **2** and **3**. Consequently, comparing to **2** and **3**, **1** exhibits much larger steric resistance on both sides of the porphyrin ring. This structural difference leads to their different electrocatalytic HER behaviors. By studying 1e-reduced forms of **1** and **2**, we show that in both cases, singly reduced Ni porphyrins can react with trifluoroacetic acid (TFA) to form Ni–H, but their subsequent H–H bond forming pathways are regulated by porphyrin steric effects. This work represents an unparalleled example of controlling HER mechanisms by tuning steric effects of molecular catalysts.

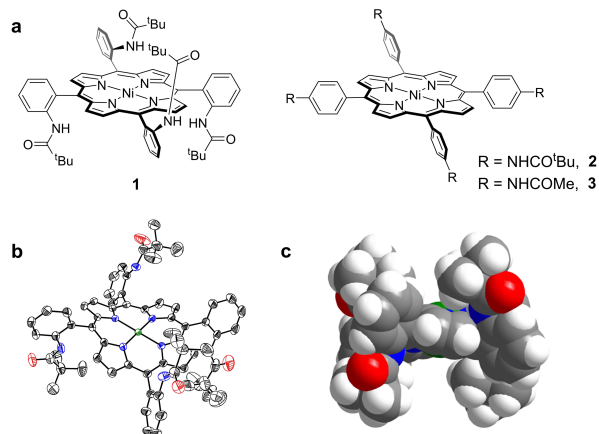


Figure 2. (a) Molecular structures of Ni porphyrins **1**, **2**, and **3**. (b) Thermal-ellipsoid plot of the X-ray structure of **1** (50% probability). Hydrogen atoms are omitted for clarity. (c) Space-filling diagram of **1**.

[a] Dr. X. J. Guo,^[*] N. Wang,^[*] Dr. X. L. Li, S. P. Ding, G. L. Xu, Prof. Dr. W. Zhang, Prof. Dr. R. Cao
Key Laboratory of Applied Surface and Colloid Chemistry, Ministry of Education, School of Chemistry and Chemical Engineering, Shaanxi Normal University, Xi'an 710119, China
E-mail: ruicao@ruc.edu.cn

[b] Z. Y. Zhang
Chemistry Research Laboratory, Department of Chemistry, University of Oxford, Mansfield Road, Oxford, OX1 3TA, UK

[c] J. P. Zhao, W. J. Ren, Prof. Dr. J. F. Li
College of Materials Science and Optoelectronic Technology, University of Chinese Academy of Science, Beijing 101408, China

[d] Prof. Dr. U.-P. Apfel
Ruhr Universität Bochum, Fakultät für Chemie und Biochemie, Anorganische Chemie I Universitätsstrasse 150, 44801 Bochum, Germany

[e] Prof. Dr. U.-P. Apfel
Fraunhofer UMSICHT, Osterfelder Strasse 3, 46047 Oberhausen, Germany

[*] These authors contributed equally to this work.

Supporting information for this article is given via a link at the end of the document.

Ni porphyrins **1-3** were designed and synthesized (detailed synthetic procedures are described in Supporting Information). These porphyrins have *meso*-phenyl groups with similar amido substituents at *ortho*-positions for **1** and *para*-positions for **2** and **3**. For **1**, bulky pivalamido substituents provide sufficient steric resistance to hinder free rotation of the phenyl groups, leading to different spatial isomers (Scheme S2). The $\alpha\beta\alpha\beta$ isomer is more favorable thermodynamically and can be enriched.

Complex **1** is structurally characterized (Figure 2b), showing the desired $\alpha\beta\alpha\beta$ configuration with the four pivalamido groups having alternating upward and downward orientations. The Ni atom is located at the porphyrin center, and the Ni^{II} oxidation state is suggested by four Ni–N bonds of 1.913(2)–1.928(2) Å and by charge balance calculation. Both sides of the porphyrin macrocycle are sterically protected (Figure 2c). The purity and identity of **1** are further confirmed by NMR (Figure S2) and high-resolution mass spectrometry (Figure S3). Complexes **2** and **3** were also structurally characterized (Figure S10), showing small steric resistance at the direction perpendicular to porphyrin rings.

The cyclic voltammogram (CV) of **1** in dimethylformamide (DMF, 0.1 M Bu₄NPF₆) under N₂ shows two reversible 1e-redox waves at –1.54 and –2.12 V vs ferrocene (Figure 3a and S11, all potentials reported in this work are referenced to ferrocene). The peak currents display linear correlation with square root of scan rates (Figure S11), indicating diffusion-controlled processes. For simplicity, we assign these two redox waves to be $1^{0/1-}$ and $1^{1-/2-}$, respectively. The CVs of **2** and **3** display reversible 1e-reduction wave at –1.63 and –1.64 V, respectively (Figure 3a). Both **1** and **2** have pivalamido units substituted at the *meso*-phenyl groups. However, X-ray structure analysis shows that the porphyrin ring of **1** is substantially saddled due to the steric hinderance of bulky *ortho*-substituents, while the porphyrin ring of **2** is almost planar because the pivalamido units are *para*-substituted. This severe distortion from the planar geometry is known to affect electronic structure of metal porphyrins,^[45] leading to 90 mV anodic shift of the first reduction wave of **1** as compared to **2** in electrochemical measurements.

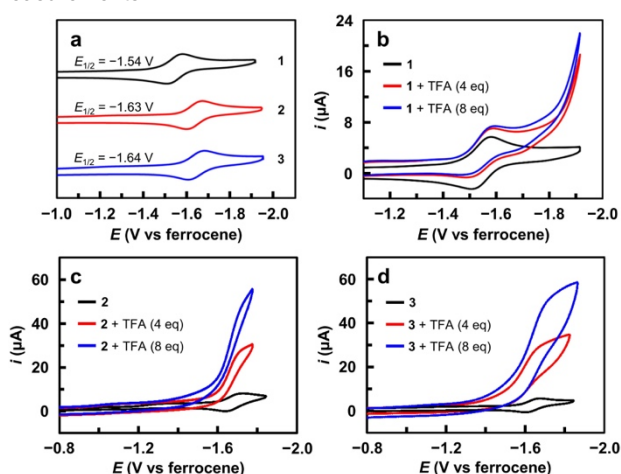


Figure 3. (a) CVs of Ni porphyrins **1**, **2**, and **3** in DMF. CVs of **1** (b), **2** (c), and **3** (d) in DMF with addition of TFA. Conditions: 0.5 mM catalyst, glassy carbon working electrode, 100 mV s⁻¹ scan rate, 23 °C.

The electrocatalytic HER features of **1-3** were investigated in DMF under N₂ with addition of TFA. As shown in Figure 3b, in the presence of TFA, the $1^{0/1-}$ wave loses the reversibility, and a new catalytic wave, which is well behind the $1^{0/1-}$ wave, appears and increases in intensity with increasing TFA. Note that the CV of TFA alone shows very small current under identical conditions (Figure S12). These results suggest catalytic HER with **1**, and also suggest that although 1^- is protonated with TFA, further reduction of the resulting species under more negative potentials is required for catalysis. Unlike **1**, the first reduction wave of **2** and **3** becomes a large catalytic one upon addition of TFA (Figure 3c and 3d, respectively). It is necessary to note that the different electrocatalytic behavior of **1** is not caused by the anodic shift of its reduction wave, since Ni TFPF has the first reduction wave at –1.28 V, which becomes a large catalytic one with addition of TFA (Figure S14).^[43] This HER behavior is similar to that of **2** and **3**. Therefore, these results suggest that the different HER behaviors of **1-3** are attributed to their different steric effects: **1** has large steric resistance on both sides of the porphyrin ring, while **2** and **3** have small steric resistance at the direction perpendicular to the porphyrin ring.

The molecular nature and catalytic stability were confirmed. For **1** and **2**, their catalytic currents show first-order dependence on the concentrations of TFA (Figure S15) and catalyst (Figure S16). During bulk electrolysis with TFA, the currents maintained constant, the accumulated charges increased linearly with time, and their UV-vis spectra after electrolysis showed almost no changes as compared to those before electrolysis (Figure S17 for **1** and Figure S18 for **2**). All these results confirm that both **1** and **2** are stable by functioning as HER catalysts.

In order to understand HER mechanisms, we generated 1^- and 2^- and studied their reaction with TFA. As shown in Figure 4a, upon 1e reduction of **1** with one equivalent of KC₈, the Soret band at 417 nm and the Q band at 529 nm decrease in intensity, and meanwhile new peaks at 448, 543 and 589 nm appear. The changes are accompanied with isosbestic points at 350, 405, 435, 517 and 538 nm (Figure 4b), suggesting clean conversion from **1** to 1^- . During the reduction, the Soret band does not show a redshift, and the absorption in the 550–700 nm range does not increase, suggesting a metal-centered reduction to give Ni^I.^[43,46] In electron paramagnetic resonance (EPR) analysis, **1** with a Ni^{II} state is EPR-silent, while 1^- shows typical Ni^I signals under the liquid helium temperature (Figure 4d),^[46] confirming a metal-centered reduction.

Addition of excess TFA to 1^- at –20 °C leads to a new UV-vis spectrum (Figure 4a), and during this process, well-defined isosbestic points at 392, 431 and 495 nm are observed (Figure 4c). No broad and intense absorption peaks in the 600–800 nm range, which are characteristic for phlorins,^[47-49] are observed in UV-vis measurement. This result argues against the protonation at the porphyrin ring. In addition, the EPR of the resulted species shows significantly large g values, which are indicative of a Ni^{III} state (Figure 4d).^[50-52] It is worth noting that the tiny signal with g = 1.99 is due to residual 1^- . Based on these results, we can propose that the oxidative protonation of Ni^I with TFA gives Ni^{III}–H,^[53] which has insufficient basicity for heterolytic protonolysis with TFA.^[43,54] This Ni^{III}–H of **1** is also unlikely to undergo bimetallic homolysis due to the large steric resistance on both sides of the porphyrin ring. Thus, further reduction of

this hydride under more negative potential is required for catalysis (Figure 3b). Further reduction of metal hydrides to make more active ones for heterolytic HER has been proposed previously.^[37,55-58] Note that 1^- shows no changes under N_2 and can be oxidized with O_2 to regenerate 1 (Figure S19). This result suggests that 1^- has sufficient stability for these studies.

Moreover, 1^- can be reduced by one more electron with KC_8 to give 1^{2-} . This process displays isosbestic points at 392, 426, 494 and 530 nm in UV-vis (Figure S20). EPR of 1^{2-} displays no obvious signals (Figure S20), suggesting metal-based reduction to give Ni^0 . Addition of excess TFA to 1^{2-} fully recovers 1 (Figure S20). This result suggests that the oxidative protonation of 1^{2-} produces $Ni^{II}-H$ and confirms that $Ni^{II}-H$ is basic enough to undergo heterolytic protonolysis with TFA to make H_2 .

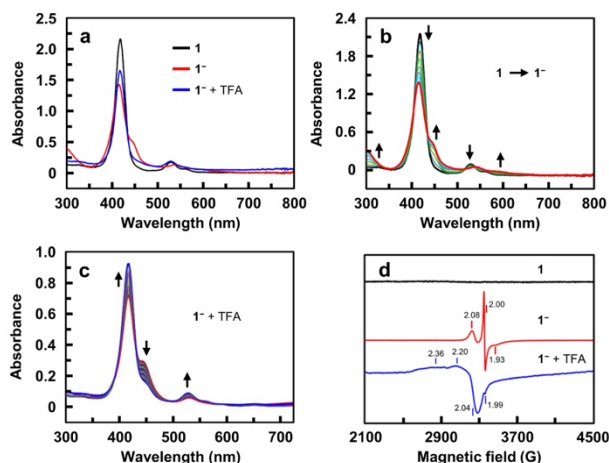


Figure 4. (a) UV-vis spectra of 1 , 1^- , and 1^- with added TFA in DMF. (b) UV-vis change upon 1e-reduction of 1 . (c) UV-vis change of 1^- upon adding excess TFA as monitored by stopped-flow technique at $-20^\circ C$. (d) Liquid-helium temperature EPR spectra of 1 , 1^- , and 1^- with addition of excess TFA.

Complex 2 can also be singly and doubly reduced. Upon 1e-reduction, the Soret band at 420 nm decreases, while absorption at 472 and 606 nm increase, displaying isosbestic points at 411 and 439 nm (Figure 5a and 5b). Unlike 1^- , intermediate 2^- has considerably enhanced absorption in the 550-650 nm range, suggesting that it is better described as a Ni^I species with some Ni^{II} porphyrin π -anion radical character. This is supported by EPR analysis of 2^- , showing increased porphyrin π -anion radical character (Figure 5d).^[46] Addition of TFA to 2^- leads to complete recovery of the UV-vis spectrum of 2 with isosbestic points at 379, 441 and 488 nm (Figure 5a and 5c). No intermediate can be identified in stopped-flow studies even at $-20^\circ C$ (the lowest temperature of the instrument). The resulted solution is EPR-silent (Figure 5d), which is consistent with the formation of 2 . On the basis of these results, we propose that the oxidative protonation of 2^- to make $Ni^{III}-H$ is the rate-limiting step and subsequent bimolecular homolysis of $Ni^{III}-H$ occurs immediately to make H_2 and 2 . This is consistent with electrocatalytic studies, showing that the reduction wave of $2^{0/1-}$ becomes a large catalytic wave with TFA and catalytic currents increases linearly with 2 (Figure S16b).

The reduction of 2^- by one more equivalent of KC_8 displays isosbestic points at 399 and 435 nm in UV-vis (Figure S21).

EPR of 2^{2-} shows no obvious signals (Figure S21), supporting a metal-based reduction. Addition of excess TFA to 2^{2-} also leads to the complete regeneration of 2 (Figure S21). This behavior indicates the formation of $Ni^{II}-H$, which can undergo heterolytic protonolysis with TFA to release H_2 and the Ni^{II} porphyrin.

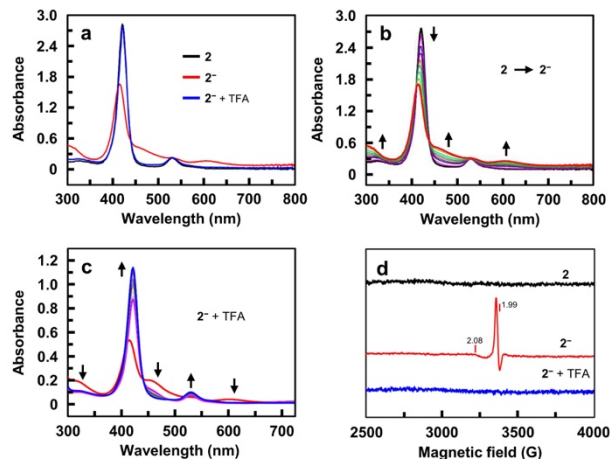


Figure 5. (a) UV-vis spectra of 2 , 2^- , and 2^- with added TFA in DMF. (b) UV-vis change upon 1e-reduction of 2 . (c) UV-vis change of 2^- upon adding excess TFA as monitored by stopped-flow technique at $-20^\circ C$. (d) Liquid-helium temperature EPR spectra of 2 , 2^- , and 2^- with addition of excess TFA.

To further confirm the homolytic HER from $Ni^{III}-H$ of 2 , we studied the hydride transfer reaction between $NaHB(OAc)_3$ and Ni^{III} . The hydride transfer ability of $NaHB(OAc)_3$ was confirmed by its reaction with Ga^{III} TFPF, giving the known $Ga^{III}-H$ with the same electronic absorption spectrum as we reported previously (Figure S22).^[26] Notably, no reduction of Ga^{III} porphyrin and no H_2 evolution were observed during this process. Next, the CV of 2 shows a quasi-reversible 1e oxidation wave at 0.51 V (Figure S23b). Consequently, we can electro-oxidize 2 to make 2^+ . As shown in Figure S24a, upon 1e oxidation, the Soret band at 420 nm and the Q band at 532 nm decrease in intensity, while the absorption at 464 nm increases. Because absorption in the 550-700 nm range does not increase, this result suggests a metal-centered oxidation. Significantly, subsequent reaction of 2^+ with one equivalent of $NaHB(OAc)_3$ fully recovers 2 (Figure S24b and S24c), and during this process, a total of 0.40 equivalent of H_2 was evolved (Figure S24d). This gives a yield 79% for homolytic HER. Note that the reaction of 2 with $NaHB(OAc)_3$ gives no H_2 and no change in UV-vis spectroscopy (Figure S25), confirming that $NaHB(OAc)_3$ is not able to reduce 2 . This observation excludes the possibility that 2^+ is first reduced by $NaHB(OAc)_3$ to generate 2^- and protons, which then undergo HER. Electro-oxidation of 1 to 1^+ displayed similar changes in UV-vis spectroscopy (Figure S26a). However, unlike 2^+ , the reaction of 1^+ and $NaHB(OAc)_3$ gave a UV-vis spectrum, which was not comparable to that of 1 but was almost identical to that obtained by adding TFA to 1^- (Figure S26b and S26c). Therefore, we can assign the resulting species as the $Ni^{III}-H$ of 1 . Importantly, no H_2 was evolved during this reaction (Figure S26d). These results suggest that (1) $Ni^{III}-H$ is actually involved in the HER for both 1 and 2 and (2) $Ni^{III}-H$ of 2 can undergo homolytic HER.

Moreover, we measured the CV of **1** with addition of one equivalent of TFA. A small but significant reduction peak, which is behind and separated from the $1^{0/1-}$ reduction wave, appears at $E_{p,c} = -1.77$ V (Figure S27). This reduction event is very close to the onset of catalytic HER wave with **1**. Thus, we attributed this reduction wave to the 1e-reduction of $Ni^{III}-H$ and proposed that this reduction made the hydride more active for heterolytic protonolysis with TFA. Unlike **1**, with one equivalent of TFA, the CV of **2** shows a catalytic wave at the $2^{0/1-}$ reduction potential and a new reduction wave at $E_{p,c} = -1.93$ V, which is well behind and separated from the $2^{0/1-}$ wave (Figure S28). Based on these results, we can attribute this new reduction wave at $E_{p,c} = -1.93$ V to the reduction of $Ni^{III}-H$ of **2**.

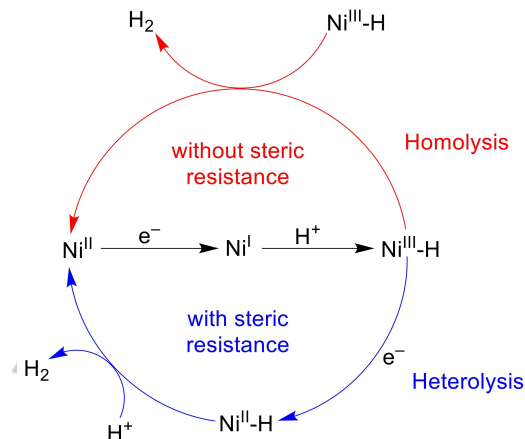
Taking these results together, we can make two conclusions. First, the protonation occurs at the Ni site of **1**⁻ and **2**⁻. Dissimilar electrocatalytic behaviors of **1** and **2** strongly argue against the protonation at *meso*-C sites, as proposed by theoretical studies on hangman porphyrins.^[59] The reason is that pivalamido groups are substituted at the *ortho*- and *para*-positions for **1** and **2**, respectively, and thus their *meso*-C sites are expected to have similar electronic and steric properties. This is not consistent with their dissimilar electrocatalytic HER behaviors. In addition, the hydride species formed by **1**⁻ with TFA does not show broad and intense absorption peaks in the 600-800 nm range in UV-vis spectrum, which are characteristic for phlorins, and shows EPR signals for Ni^{III} . These results support the protonation at the Ni site. More importantly, the hydride transfer from $NaHB(OAc)_3$ to **1**⁺ gives UV-vis spectrum of $Ni^{III}-H$, and the reaction between $NaHB(OAc)_3$ and **2**⁺ fully recovers **2** and generates H_2 . All these reaction features of **1** and **2** are consistent with the involvement of Ni-based hydride intermediates in the HER.

Second, bimolecular homolysis of $Ni^{III}-H$ is involved in the HER with **2**. After oxidative protonation of **2**⁻ with TFA, there are two possible pathways for the resulted $Ni^{III}-H$ species to evolve H_2 : it can undergo homolytic HER or it requires further reduction by residual **2**⁻ to become active for heterolytic protonolysis with TFA. However, the reduction potential of $Ni^{III}-H$ is more negative than the $2^{0/1-}$ redox potential by 300 mV. Thus, **2**⁻ is not able to reduce $Ni^{III}-H$. Consequently, further reduction of $Ni^{III}-H$ by **2**⁻ to become active for HER is not likely. In addition, the reaction of **2**⁻ with one equivalent of $NaHB(OAc)_3$ can fully recovers **2** and generate H_2 with a yield of 79%. This is a strong support of the homolytic HER from $Ni^{III}-H$ as no protons exist in this system.

Based on results from electrochemical and chemical studies, we demonstrate that **1**⁻ and **2**⁻ show different mechanisms to evolve H_2 when treated with TFA (Scheme 1). Because of bulky pivalamido groups located on both sides of the porphyrin ring of **1**, the bimolecular homolytic mechanism of $Ni^{III}-H$ of **1** is blocked. As a result, $Ni^{III}-H$ of **1** requires further 1e-reduction to become more active for the heterolytic protonolysis with TFA. In sharp contrast, because of the presence of small steric resistance at the direction perpendicular to the porphyrin ring of **2**, the $Ni^{III}-H$ generated from **2**⁻ and TFA can undergo bimetallic homolysis to make H_2 . Moreover, unlike singly reduced forms, doubly reduced **1** and **2** are able to reduce TFA to yield $Ni^{II}-H$ species, and these $Ni^{II}-H$ have similar reaction features to undergo heterolytic protonolysis with TFA to generate H_2 . This further underlines the dissimilar reaction features of $Ni^{III}-H$ forms obtained from **1** and

2, which is also supportive of the involvement of bimolecular homolytic mechanism in the HER with **2**.

Scheme 1. Proposed catalytic HER mechanisms with **1** and **2**, showing the switching between homolytic (red) and heterolytic (blue) pathways regulated by the steric effects of Ni porphyrins.



In conclusion, we herein report that Ni porphyrins, which have distinct steric effects by introducing bulky amido moieties to *ortho*- or *para*-positions of *meso*-phenyl groups, display different HER behaviors. Although 1e-reduced Ni porphyrins are able to react with TFA, the resulting hydride intermediate – depending on the steric resistance along the perpendicular direction of porphyrin rings – will either undergo direct bimetallic homolysis to evolve H_2 or require further reduction for heterolytic protonolysis. Such switching between homolytic and heterolytic HER pathways via the regulation of molecular steric effects is unprecedented. Our results also demonstrate that for reduced Ni porphyrins, the oxidative protonation occurs at Ni sites rather than *meso*-C sites. This work improves the understanding of the HER mechanisms and provides valuable insights into catalyst design with more consideration from steric effects.

Acknowledgements

We are grateful for support from the “Thousand Talents Program” of China, Fok Ying-Tong Education Foundation for Outstanding Young Teachers in University, National Natural Science Foundation of China (Grants 21101170, 21573139, and 21773146), Fundamental Research Funds for the Central Universities, and Research Funds of Shaanxi Normal University. U.-P. A. is grateful for the financial support by the Deutsche Forschungsgemeinschaft (Emmy Noether grant AP242/2-1, under Germany’s Excellence Strategy – EXC 2033 – 390677874 – RESOLV) and the Fraunhofer Internal Programs under Grant No. Attract 097-602175.

Keywords: steric effect • hydrogen evolution • homolytic • heterolytic • nickel porphyrin

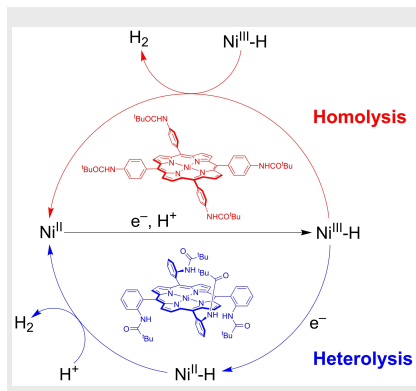
[1] N. Kaeffer, M. Chavarot-Kerlidou, V. Artero, *Acc. Chem. Res.* **2015**, *48*, 1286-1295.

- [2] S. Fukuzumi, Y.-M. Lee, W. Nam, *Coord. Chem. Rev.* **2018**, *355*, 54-73.
- [3] G. Berggren, A. Adamska, C. Lambert, T. R. Simmons, J. Esselborn, M. Atta, S. Gambarelli, J. M. Mouesca, E. Reijerse, W. Lubitz, T. Happe, V. Artero, M. Fontecave, *Nature* **2013**, *499*, 66-69.
- [4] M. L. Helm, M. P. Stewart, R. M. Bullock, M. R. DuBois, D. L. DuBois, *Science* **2011**, *333*, 863-866.
- [5] H. I. Karunadasa, C. J. Chang, J. R. Long, *Nature* **2010**, *464*, 1329-1333.
- [6] J. L. Dempsey, B. S. Brunschwig, J. R. Winkler, H. B. Gray, *Acc. Chem. Res.* **2009**, *42*, 1995-2004.
- [7] M. R. DuBois, D. L. DuBois, *Chem. Soc. Rev.* **2009**, *38*, 62-72.
- [8] R. Tatematsu, T. Inomata, T. Ozawa, H. Masuda, *Angew. Chem. Int. Ed.* **2016**, *55*, 5247-5250.
- [9] C. Tsay, J. Y. Yang, *J. Am. Chem. Soc.* **2016**, *138*, 14174-14177.
- [10] K. Koshiba, K. Yamauchi, K. Sakai, *Angew. Chem. Int. Ed.* **2017**, *56*, 4247-4251.
- [11] E. S. Andreiadis, P. A. Jacques, P. D. Tran, A. Leyris, M. Chavart-Kerlidou, B. Joussemme, M. Matheron, J. Pécaut, S. Palacin, M. Fontecave, V. Artero, *Nat. Chem.* **2013**, *5*, 48-53.
- [12] D. Brazzolotto, L. K. Wang, H. Tang, M. Gennari, N. Queyriaux, C. Philouze, S. Demeshko, F. Meyer, M. Orio, V. Artero, M. B. Hall, C. Duboc, *ACS Catal.* **2018**, *8*, 10658-10667.
- [13] J. Warnan, J. Willkomm, J. N. Ng, R. Godin, S. Prantl, J. R. Durrant, E. Reisner, *Chem. Sci.* **2017**, *8*, 3070-3079.
- [14] A. M. Appel, D. H. Pool, M. O'Hagan, W. J. Shaw, J. Y. Yang, M. R. DuBois, D. L. DuBois, R. M. Bullock, *ACS Catal.* **2011**, *1*, 777-785.
- [15] C. C. L. McCrory, C. Uyeda, J. C. Peters, *J. Am. Chem. Soc.* **2012**, *134*, 3164-3170.
- [16] J. G. Kleingardner, B. Kandemir, K. L. Bren, *J. Am. Chem. Soc.* **2014**, *136*, 4-7.
- [17] J. P. Porcher, T. Fogeron, M. Gomez-Mingot, E. Derat, L. M. Chamoreau, Y. Li, M. Fontecave, *Angew. Chem. Int. Ed.* **2015**, *54*, 14090-14093.
- [18] U. J. Kilgore, J. A. S. Roberts, D. H. Pool, A. M. Appel, M. P. Stewart, M. R. DuBois, W. G. Dougherty, W. S. Kassel, R. M. Bullock, D. L. DuBois, *J. Am. Chem. Soc.* **2011**, *133*, 5861-5872.
- [19] E. J. Thompson, L. A. Berben, *Angew. Chem. Int. Ed.* **2015**, *54*, 11642-11646.
- [20] Z.-Y. Wu, T. Wang, Y.-S. Meng, Y. Rao, B.-W. Wang, J. Zheng, S. Gao, J.-L. Zhang, *Chem. Sci.* **2017**, *8*, 5953-5961.
- [21] A. Mahammed, B. Mondal, A. Rana, A. Dey, Z. Gross, *Chem. Commun.* **2014**, *50*, 2725-2727.
- [22] W. Zhang, W. Z. Lai, R. Cao, *Chem. Rev.* **2017**, *117*, 3717-3797.
- [23] H. T. Lei, X. L. Li, J. Meng, H. Q. Zheng, W. Zhang, R. Cao, *ACS Catal.* **2019**, *9*, 4320-4344.
- [24] F. Möller, S. Piontek, R. G. Miller, U. P. Apfel, *Chem. Eur. J.* **2018**, *24*, 1471-1493.
- [25] X. L. Li, H. T. Lei, J. Y. Liu, X. L. Zhao, S. P. Ding, Z. Y. Zhang, X. X. Tao, W. Zhang, W. C. Wang, X. H. Zheng, R. Cao, *Angew. Chem. Int. Ed.* **2018**, *57*, 15070-15075.
- [26] N. Wang, H. T. Lei, Z. Y. Zhang, J. F. Li, W. Zhang, R. Cao, *Chem. Sci.* **2019**, *10*, 2308-2314.
- [27] J. B. Jiang, K. L. Materna, S. Hedström, K. R. Yang, R. H. Crabtree, V. S. Batista, G. W. Brudvig, *Angew. Chem. Int. Ed.* **2017**, *56*, 9111-9115.
- [28] A. Z. Haddad, B. D. Garabato, P. M. Kozlowski, R. M. Buchanan, C. A. Grapperhaus, *J. Am. Chem. Soc.* **2016**, *138*, 7844-7847.
- [29] D. Khusnutdinova, B. L. Wadsworth, M. Flores, A. M. Beiler, E. A. R. Cruz, Y. Zenkov, G. F. Moore, *ACS Catal.* **2018**, *8*, 9888-9898.
- [30] A. G. Maher, G. Passard, D. K. Dogutan, R. L. Halbach, B. L. Anderson, C. J. Gagliardi, M. Taniguchi, J. S. Lindsey, D. G. Nocera, *ACS Catal.* **2017**, *7*, 3597-3606.
- [31] S. Roy, Z. H. Huang, A. Bhunia, A. Castner, A. K. Gupta, X. D. Zou, S. Ott, *J. Am. Chem. Soc.* **2019**, *141*, 15942-15950.
- [32] B. P. Biswal, H. A. Vignolo-González, T. Banerjee, L. Grunenberg, G. Savasci, K. Gottschling, J. Nuss, C. Ochsenfeld, B. V. Lotsch, *J. Am. Chem. Soc.* **2019**, *141*, 11082-11092.
- [33] J.-W. Wang, K. Yamauchi, H.-H. Huang, J.-K. Sun, Z.-M. Luo, D.-C. Zhong, T.-B. Lu, K. Sakai, *Angew. Chem. Int. Ed.* **2019**, *58*, 10923-10927.
- [34] V. Firpo, J. M. Le, V. Pavone, A. Lombardi, K. L. Bren, *Chem. Sci.* **2018**, *9*, 8582-8589.
- [35] M. E. Ahmed, S. Chattopadhyay, L. Wang, D. Brazzolotto, D. Pramanik, D. Aldakov, J. Fize, A. Morozan, M. Gennari, C. Duboc, A. Dey, V. Artero, *Angew. Chem. Int. Ed.* **2018**, *57*, 16001-16004.
- [36] J. A. Buss, M. Hirahara, Y. Ueda, T. Agapie, *Angew. Chem. Int. Ed.* **2018**, *57*, 16329-16333.
- [37] S. C. Marinescu, J. R. Winkler, H. B. Gray, *Proc. Natl. Acad. Sci. USA* **2012**, *109*, 15127-15131.
- [38] C. N. Valdez, J. L. Dempsey, B. S. Brunschwig, J. R. Winkler, H. B. Gray, *Proc. Natl. Acad. Sci. USA* **2012**, *109*, 15589-15593.
- [39] C. H. Lee, D. K. Dogutan, D. G. Nocera, *J. Am. Chem. Soc.* **2011**, *133*, 8775-8777.
- [40] P. Wang, G. C. Liang, M. R. Reddy, M. Long, K. Driskill, C. Lyons, B. Donnadiou, J. C. Bollinger, C. E. Webster, X. Zhao, *J. Am. Chem. Soc.* **2018**, *140*, 9219-9229.
- [41] N. Elgrishi, D. A. Kurtz, J. L. Dempsey, *J. Am. Chem. Soc.* **2017**, *139*, 239-244.
- [42] M. J. Rose, H. B. Gray, J. R. Winkler, *J. Am. Chem. Soc.* **2012**, *134*, 8310-8313.
- [43] Y. Z. Han, H. Y. Fang, H. Z. Jing, H. L. Sun, H. T. Lei, W. Z. Lai, R. Cao, *Angew. Chem. Int. Ed.* **2016**, *55*, 5457-5462.
- [44] S. Ramakrishnan, S. Chakraborty, W. W. Brennessel, C. E. D. Chidsey, W. D. Jones, *Chem. Sci.* **2016**, *7*, 117-127.
- [45] K. E. Thomas, A. B. Alemayehu, J. Conradie, C. M. Beavers, A. Ghosh, *Acc. Chem. Res.* **2012**, *45*, 1203-1214.
- [46] K. M. Kadish, M. M. Franzen, B. C. Han, C. Araullo-McAdams, D. Sazou, *J. Am. Chem. Soc.* **1991**, *113*, 512-517.
- [47] A. S. Aslam, J. H. Hong, J. H. Shin, D. G. Cho, *Angew. Chem. Int. Ed.* **2017**, *56*, 16247-16251.
- [48] G. X. Su, Q. Z. Li, M. Ishida, C. J. Li, F. Sha, X. Y. Wu, L. Wang, G. Baryshnikov, D. W. Li, H. Ågren, H. Furuta, Y. S. Xie, *Angew. Chem. Int. Ed.* **2020**, *59*, 1537-1541.
- [49] A. J. Pistner, D. A. Lutterman, M. J. Ghidui, Y. Z. Ma, J. Rosenthal, *J. Am. Chem. Soc.* **2013**, *135*, 6601-6607.
- [50] Y. Shimazaki, F. Tani, K. Fukui, Y. Naruta, O. Yamauchi, *J. Am. Chem. Soc.* **2003**, *125*, 10512-10513.
- [51] M. Gennari, M. Orio, J. Pécaut, E. Bothe, F. Neese, M.-N. Collomb, C. Duboc, *Inorg. Chem.* **2011**, *50*, 3707-3716.
- [52] C.-W. Chiang, Y.-L. Chu, H.-L. Chen, T.-S. Kuo, W.-Z. Lee, *Chem. Eur. J.* **2014**, *20*, 6283-6286.
- [53] N. A. Eberhardt, H. R. Guan, *Chem. Rev.* **2016**, *116*, 8373-8426.
- [54] R. H. Morris, *Chem. Rev.* **2016**, *116*, 8588-8654.
- [55] M. E. Carroll, B. E. Barton, T. B. Rauchfuss, P. J. Carroll, *J. Am. Chem. Soc.* **2012**, *134*, 18843-18852.
- [56] J. T. Muckerman, E. Fujita, *Chem. Commun.* **2011**, *47*, 12456-12458.
- [57] O. A. Ulloa, M. T. Huynh, C. P. Richers, J. A. Bertke, M. J. Nilges, S. Hammes-Schiffer, T. B. Rauchfuss, *J. Am. Chem. Soc.* **2016**, *138*, 9234-9245.
- [58] H. T. Lei, H. Y. Fang, Y. Z. Han, W. Z. Lai, X. F. Fu, R. Cao, *ACS Catal.* **2015**, *5*, 5145-5153.
- [59] B. H. Solis, A. G. Maher, D. K. Dogutan, D. G. Nocera, S. Hammes-Schiffer, *Proc. Natl. Acad. Sci. USA* **2016**, *113*, 485-492.

Entry for the Table of Contents (Please choose one layout)

COMMUNICATION

Homolytic vs heterolytic HER: Ni porphyrins with distinct steric effects by introducing amido units to *ortho*- or *para*-positions of *meso*-phenyl groups display different catalytic HER behaviors. Depending on steric resistance on both sides of porphyrin rings, hydride intermediates, formed through the oxidative protonation of 1e-reduced Ni porphyrins, either undergo bimetallic homolysis or is required to be further reduced for heterolytic protonolysis to evolve H₂.



Xiaojun Guo, Ni Wang, Xialiang Li, Zongyao Zhang, Jianping Zhao, Wanjie Ren, Shuping Ding, Gelun Xu, Jianfeng Li, Ulf-Peter Apfel, Wei Zhang, and Rui Cao*

Page No. – Page No.

Homolytic versus Heterolytic Hydrogen Evolution Reaction Steered via Steric Effect

Accepted Manuscript